Sensitivity of Internal-Tide Generation to Stratification and Its Implication for Deep Overturning Circulations

VEIT LÜSCHOW[a] AND JIN-SONG VON STORCH[a,b]

[a] *Max-Planck Institute for Meteorology, Hamburg, Germany*
[b] *Center for Earth System Research and Sustainability (CEN), University of Hamburg, Hamburg, Germany*

ABSTRACT: The simple scaling relation for internal-tide generation proposed by Jayne and St. Laurent is widely used for parameterizing turbulent mixing induced by breaking of internal tides. Based on the internal-tide generation derived from a 0.1° ocean general circulation model, we show that depending on which stratification is used, this relation produces different vertical distributions of internal-tide generation. When using the buoyancy frequency at the seafloor, which is a common practice, the scaling relation produces, relative to the model, too-strong internal-tide generation in the upper 2000 m and too-weak internal-tide generation in the lower 2000 m. Moreover, the different vertical distributions in the different ocean basins, characterized by a generally decreasing internal tide generation with increasing depth in the Indo-Pacific but not-decreasing or even increasing internal tide generation with increasing depth in the upper 3000 m of the Atlantic, cannot be captured when using bottom stratification. These unsatisfactory features can be easily removed by replacing the buoyancy frequency at the seafloor by a buoyancy frequency averaged over a large part of the water column. To our knowledge, this sensitivity to stratification has not been explicitly quantified for the global ocean. Because of this sensitivity, the scaling relation of Jayne and St. Laurent should be used with an averaged stratification to ensure a more adequate representation of turbulent diffusivity due to tidal mixing and water mass transformation in the deep oceans.

KEYWORDS: Mixing; Oceanic waves; Ocean models; Parameterization

1. Introduction

Turbulent mixing due to breaking of internal tides is thought to provide much of the mechanical energy needed to maintain the interior stratification and the overturning circulation in the ocean (Munk and Wunsch 1998; Wunsch and Ferrari 2004). Thus, most of the state-of-the-art ocean general circulation models (GCMs) employ a parameterization of tidal mixing (Simmons et al. 2004; Jayne 2009; Exarchou et al. 2012; Danabasoglu et al. 2012; Dunne et al. 2012; Madec and NEMO Team 2016; Sasaki et al. 2020). The widely used one is that proposed by St. Laurent et al. (2002). There the near-field portion of the total tidal mixing is described by a diffusivity that is proportional to an internal tide energy flux E, which results from barotropic tides, and the local dissipation efficiency q, which specifies how much of E is directly dissipated at the generation sites. The flux E is also referred to as internal tide generation. In St. Laurent et al. (2002), E is approximated by a scaling relation derived by Jayne and St. Laurent (2001) based on linear wave theory. This E, hereafter referred to as E_{JSL}, takes the form

$$E_{JSL} = \frac{1}{2}\rho_o h^2 \kappa N |\mathbf{U}_H|^2, \tag{1}$$

where ρ_o denotes a reference density of seawater, h^2 measures the roughness of the bathymetry, κ is the wavenumber parameter,

N is buoyancy frequency. The E_{JSL} is used not only in the simple scheme of St. Laurent et al. (2002), that is implemented in many state-of-the-art OGCMs (such as those cited above), but also as the source of internal wave energy at seafloor in the more advanced and newly developed mixing scheme Internal Wave Dissipation, Energy and Mixing (IDEMIX; Olbers and Eden 2013), that has been recently implemented in the Community Climate System Model, version 4 (CCSM4; Nielsen et al. 2018). Despite the wide use, E_{JSL} has, to our knowledge, not been directly evaluated. This paper aims to fill this gap by evaluating E_{JSL} against the internal tide generation simulated by a realistic ocean GCM. The goal is to identify the possible problem associated with using E_{JSL} and to propose a remedy to solve this problem, thereby improving the parameterization of St. Laurent et al. (2002) and at the same time retaining its simplicity.

The E_{JSL} may suffer from at least two problems. The first one is related to the ad hoc nature of E_{JSL}: E_{JSL} relies on the buoyancy frequency at the seafloor—a feature of WKB-approximated linear wave solutions—rather than on the stratification throughout the water column that is needed to derive the exact linear wave solutions. The second problem is related to assumptions underlying linear wave theory that are not satisfied everywhere in the real ocean. These assumptions include that of subcritical topography, meaning that the internal tide characteristic slope must be larger than that of the bathymetry, and that of small tidal excursion, meaning that the tidal excursion must be smaller than the horizontal topographic scale. Both the ad hoc nature and the assumptions behind linear wave theory can be, at least partially, overcome by using a numerical model. We are aware that internal tide generation simulated by a numerical model may suffer from other problems arising from limited horizontal resolution, inadequate parameterization of unresolved dissipative processes,

---

Corresponding author: Jin-Song von Storch, jin-song.von.storch@mpimet.mpg.de

and other factors that lead to the model biases. We nevertheless assume that internal tide generation simulated by an ocean GCM with realistic topography forced by realistic surface fluxes and by the full luni-solar tidal potential is much closer to real internal tide generation than E_{JSL} and hence can be used for evaluating E_{JSL}. Given the scarceness of the observations and in regard to what is available to us, we evaluate E_{JSL} against that simulated in STORMTIDE2, a concurrent simulation of tide and circulation performed with the Max-Planck Institute Ocean Model (MPI-OM) at a horizontal resolution of about 0.1°. This internal tide generation is derived by Li and von Storch (2020) and will be referred to as E_{LvS}.

We note that, apart from E_{LvS}, there exist several estimates of internal tide generation, which can also be used to evaluate E_{JSL}. We have not only the estimate obtained from semianalytical solutions of linear wave equations (Nycander 2005; Falahat et al. 2014), but also the estimate obtained from another ocean model HYCOM (Buijsman et al. 2020). The main characteristics of these estimates are similar to those found in STORMTIDE2. However, there are also clear differences. The effects of some of these differences can be inferred from the recent simulations by Brüggemann et al. (2023), in which different estimates of internal tide generation were used as the bottom boundary forcing for IDEMIX. Since we want to evaluate E_{JSL} as consistently as possible, so that the difference between E_{JSL} and one of these estimates is not caused by using different stratification or different tidal velocity or different topography, we choose to stay within the framework of STORMTIDE2. A brief comparison of E_{LvS} with some of the existing estimates is given in section 5a.

The paper is organized as follows. Section 2 provides a description of STORMTIDE2 and describes the methods used for evaluating E_{JSL} against E_{LvS}. The evaluation focuses on the vertical distribution of internal tide generation, since diapycnal mixing is more closely linked to the vertical than to the horizontal distribution of internal tide generation, as the neutral density surfaces can be assumed to be nearly horizontal in the abyssal ocean (Ferrari et al. 2016). In section 3, E_{JSL} is calculated by setting N in Eq. (1) either to the buoyancy frequency at the seafloor as it is done in most applications or to a buoyancy frequency obtained by taking the vertical density profile into account. By comparing them with that obtained from E_{LvS}, the sensitivity of E_{JSL} to stratification is identified and quantified. What this sensitivity means for the water mass transformation is assessed in section 4. A comparison of E_{LvS} with some existing estimates of internal tide generation and a discussion of the relevance of the identified sensitivity for parameterizing near-field tidal mixing are given in section 5. A summary is given in section 6.

2. Methods

a. STORMTIDE2

STORMTIDE2 is a follow-up of STORMTIDE, the first 0.1° concurrent simulation of tide and circulation carried out with MPI-OM (Müller et al. 2012; Li et al. 2015, 2017), a primitive equation ocean general circulation model. Both STORMTIDE and STORMTIDE2 employ the complete luni-solar potential (Thomas et al. 2001) and are performed with the same tripolar

version of MPI-OM at a horizontal resolution of about 0.1° and the same bathymetry obtained by interpolating SRTM30 (Farr et al. 2007) on to the model grid. The 0.1° horizontal resolution corresponds to a grid size of about 11 km at the equator and down southward to the smallest grid size of 2.3 km off the Antarctic coast. The main difference between STORMTIDE2 and STORMTIDE concerns the forcing at the sea surface. While STORMTIDE is performed by restoring sea surface temperature and sea surface salinity to observed climatological values, a more realistic representation of the surface fluxes based on bulk formula is used for STORMTIDE2.

STORMTIDE2 is run using the standard parameterizations of tracer mixing and momentum dissipation due to unresolved processes (Jungclaus et al. 2013). The vertical mixing of tracers is parameterized by a modified PP scheme (Pacanowski and Philander 1981), which depends on Richardson number and includes the effect of surface winds. The isopycnal mixing is parameterized by a grid-size-dependent isopycnal diffusion (Redi 1982). The parameterization of mesoscale eddies following Gent and McWilliams (1990) is switched off, as the resolution used is fine enough to resolve a bulk of mesoscale eddies. The momentum dissipation is parameterized by a biharmonic diffusion. Tracer mixing can affect the distributions of temperature and salinity, and with that the internal tide pressure. The momentum dissipation can affect the barotropic tides. Internal tide pressure together with barotropic tides determine the internal tide generation according to Eq. (2) given below.

STORMTIDE2 produces large-scale ocean circulation and hydrology that are in good agreement with observations (Li and von Storch 2020). The performance of the barotropic tides is also satisfactory. A comparison against 102 pelagic tidal measurements reveals for the eight major tidal constituents an accuracy of 89.0% (Li and von Storch 2020) which is comparable to the accuracy achieved by STORMTIDE (Müller et al. 2012) (92.8%) and another concurrent simulation of circulation and tide carried out with an unconstrained ocean model (Arbic et al. 2004, 2010) (92.6%). Concerning low-mode internal-tide signatures, the spatial distributions of M_2 internal tide energy compare well with those obtained from STORMTIDE consistent with the filtered satellite altimeter data (Müller et al. 2012; Li et al. 2015).

In this paper, we concentrate on the internal tide generation due to the M_2 tide, the strongest tidal constituent. The value of E_{LvS} is calculated based on the known wave generation mechanism (Bell 1975): Internal tides are generated when a barotropic tide with velocity $\mathbf{U}_H$ is doing work against the pressure force (or the form drag) $\mathbf{F} = -p_{\mathrm{bot}}^i \nabla d$, where p_{bot}^i is the bottom pressure of the internal tide and d is the depth of the seafloor. The rate of work equals then $\mathbf{U}_H \cdot \mathbf{F} = -\mathbf{U}_H \cdot (p_{\mathrm{bot}}^i \nabla d)$, and E_{LvS} is the averaged rate of work

$$E_{\mathrm{LvS}} = -\overline{\mathbf{U}_H \cdot (p_{\mathrm{bot}}^i \nabla d)}, \qquad (2)$$

where the overbar indicates the average over an M_2 period. When diagnosed from STORMTIDE2, $\mathbf{U}_H$ is the M_2 barotropic tidal velocity obtained by performing the harmonic analysis on the simulated barotropic velocity. The bottom pressure of the M_2
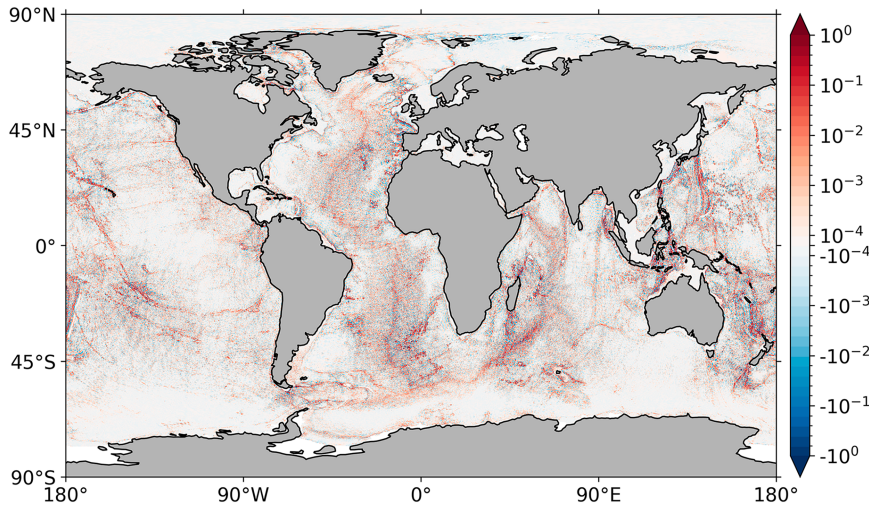
FIG. 1. E_{LvS}, the internal tide generation obtained from STORMTIDE2, plotted as a function of geographical location of generation site in a symmetric logarithmic scale. Unit is W m^{-2}.

internal tide p^i_{bot} is calculated as the deviation from the depth-averaged hydrostatic pressure at the M$_2$ frequency. The latter is derived from the density perturbations at the M$_2$ frequency found in STORMTIDE2. More details can be found in Li and von Storch (2020).

We note that being formulated as a rate of work, rather than as an energy flux, E_{LvS} may be less sensitive to the representation of dissipation than an energy flux, since the latter is more directly affected by the representation of dissipation than the former. Nevertheless, E_{LvS} may suffer from the shortcomings of the model mentioned in section 1. However, based on the overall realistic simulation of the general circulation, the mean hydrographic states, and the barotropic and internal tides (Li and von Storch 2020), we regard E_{LvS} as sufficiently accurate for the purpose of evaluating the scaling relation E_{JSL}. When not stated otherwise, the phrases "overestimate" and "underestimate" refer to a comparison of E_{JSL} with E_{LvS}.

The map of E_{LvS}, replotted using symmetric logarithmic scale in Fig. 1, shows large positive values of the internal tide generation of about 10^{-3} to 10^{-1} W m^{-2} over the ridges in the western part of the Pacific (e.g., the Sitito Iozima Ridge and Hawaiian Ridge in the western North Pacific, and around Pacific archipelagos in the western central and South Pacific), over the ridges in the western part of the Indian Ocean (e.g., the Southwest Indian Ridge), and over the Mid-Atlantic Ridge in the Atlantic Ocean. Due to the limited resolution, E_{LvS} represents essentially the generation of the first two to three modes (Li et al. 2015). The E_{LvS} is more comparable to the maps of total internal tide generation (Nycander 2005; Falahat et al. 2014; Vic et al. 2019) than to the map of generation of mode 1 internal tide only (Falahat et al. 2014; Vic et al. 2019). The E_{LvS} contains also negative values. In the analysis presented below, the negative values are removed and corrected following de Lavergne et al. (2019).

Integrated globally while excluding all regions shallower than 700 m, E_{LvS} amounts to 0.57 TW (10^{12} W). This number is somewhat higher than 0.52 TW, the estimate of internal tide

generation due to the first 10 modes obtained from Falahat et al. (2014), and 0.51 TW, the estimate of internal tide generation due to the first 10 modes obtained from Vic et al. (2019) (both for ocean deeper than 700 m). In this paper, we focus on the aspects related to vertical distribution, rather than the aspects related to the amount of the globally integrated IT generation, since the magnitude can be scaled when using the scaling relation of Jayne and St. Laurent (2001).

b. The scaling relation by Jayne and St. Laurent

The E_{JSL} given in Eq. (1) was originally used for describing the dissipation mechanism in form of a drag in barotropic tide models (Jayne and St. Laurent 2001) for the purpose of improving tides simulated by barotropic models. In the parameterization of St. Laurent et al. (2002), E_{JSL} is used as an ad hoc approximation of internal tide generation. The E_{JSL} is not a prediction of solutions of linear wave equations. These solutions can be exact, meaning obtained by solving the vertical eigenproblem using stratification throughout a water column (Llewellyn Smith and Young 2002; Nycander 2005; Falahat et al. 2014; Pollmann and Nycander 2023), or approximate, meaning obtained by applying the WKB approximation using the stratification at the sea floor without solving the vertical eigenproblem (Llewellyn Smith and Young 2002). Despite the approximative nature, E_{JSL} is extremely valuable, as it allows the formulation of an effective and yet simple tidal mixing parameterization.

We evaluate E_{JSL} in the framework of STORMTIDE2, thereby concentrating on the internal tide generation due to M$_2$ tide. For this purpose, we set $\mathbf{U}_H$ in Eq. (1) to the velocity of the M$_2$ tide diagnosed from STORMTIDE2 and using h^2 and N derived from STORMTIDE2. The way the roughness h^2 is calculated can cause differences in the simulated large-scale circulation (Exarchou et al. 2012). In the analysis carried out here, we find that the impact of the choice of how h^2 is computed is minor (not shown) as compared to the choice of

the stratification N. We compute h^2 at each grid point as the variance of the bathymetry used in STORMTIDE2. The latter is defined as the variance of the deviations from a two-dimensional surface fitted into an area, that is centered at the considered grid point and has a radius of 100 km.

The value of N is derived from the time-mean density in STORMTIDE2. But we still need to decide which stratification should this N represents. Jayne and St. Laurent (2001) suggested to choose N as the bottom stratification N_{bot}, inspired by the WKB-approximated semianalytical solutions given, e.g., in Llewellyn Smith and Young (2002). However, Zarroug et al. (2010) show that the assumed proportionality of the internal tide generation to N_{bot} is inappropriate, in particular for the low modes that carry the largest part of the internal tide energy. Instead, they suggest using a *homogenized* stratification that is the buoyancy frequency averaged over a meaningful vertical scale such as the vertical scale of the locally dominant mode of internal tides. We transfer this idea to the scaling relation of Jayne and St. Laurent (2001) and consider, besides the standard case with $N = N_{bot}$, one scenario in which we use a homogenized buoyancy frequency, $N = N_{hom}$. As vertical averaging scale for N_{hom}, we choose the first zero crossing (seen from the seafloor) of the dominant mode of the M_2 internal tide. To obtain the vertical averaging scale, we derive the vertical structures of leading modes by solving the vertical eigenvalue problem using the mean stratification in STORMTIDE2 and then pick up the dominant mode (i.e., the mode with the strongest internal tide generation) identified by Vic et al. (2019), their Fig. 4a). This procedure contains some inconsistency, as the vertical modes obtained from STORMTIDE2 could differ from those considered by Vic et al. (2019) based on observations. We assume that these differences are small, since STORMTIDE2 is able to by and large realistically simulate the general circulation and the mean hydrostatic state (Li and von Storch 2020).

The N_{hom} derived following Zarroug et al. (2010) requires resolving the eigenvalue problem and identifying the dominant mode at each grid point which conflicts with the desired simplicity of the approach by Jayne and St. Laurent (2001). To keep the calculation of N as simple as possible, we consider one more scenario in which we use a mean buoyancy frequency N_{mean} obtained by simply averaging N over the full depth except the top 300 m. The upper 300 m is excluded, because mixed layer processes should not play a role for the generation of internal waves. Note that N_{bot}, N_{hom}, and N_{mean} are determined individually at each grid point. They hence vary spatially. The E_{JSL} calculated using N_{bot}, N_{hom}, and N_{mean} will be referred to as the estimate JSL-N_{bot}, JSL-N_{hom}, and JSL-N_{mean}, respectively.

Apart from $\mathbf{U}_H$, h^2, and N, the choice has to be made for κ, which is used as a tuning parameter. In the barotropic tidal model of Jayne and St. Laurent (2001), κ was tuned to give the best fit to the observed tides. When used in the tidal mixing scheme in a GCM, e.g., in Exarchou et al. (2012), κ is often used to tune the global integral of E_{JSL}. In the present study, to ensure a meaningful comparison, we tune κ such that the total internal tide generation obtained from E_{JSL} matches 0.57 TW, the total internal tide generation below 700 m obtained from E_{LvS}. By fixing the global integral of E_{JSL}, κ must be reduced when using

N_{hom} and N_{mean} that are generally larger than N_{bot}. We obtain $\kappa = 2\pi/173$ km when using N_{bot}, $\kappa = 2\pi/616$ km when using N_{hom}, and $\kappa = 2\pi/669$ km when using N_{mean}.

c. Metric for evaluation

For both E_{JSL} and E_{LvS}, the value at a grid point represents the internal tide generation at the generation site represented by the grid point. Being located on the irregular sea floor, the internal tide generation site is a function of both horizontal location and depth. So far, the internal tide generation is mostly displayed in the form of a horizontal map, such as that shown in Fig. 1, regardless of the depth of generation sites. Here, we use the vertical distributions of the internal tide generation as the metric for our evaluation for the reasons discussed below. For the global ocean basin or an individual ocean basin, such a distribution is obtained by integrating E_{JSL} or E_{LvS} over all grid points at the seafloor in that ocean basin, that have the same depth.

One reason for considering vertical distribution arises from the idea of "abyssal recipes" (Munk 1966; Munk and Wunsch 1998) that deep energy sources are needed to match the rate of diapycnal upwelling to the rates of deep water production. Following this idea, and given that internal tide generation is the main deep energy source since other possible deep sources such as the geothermal heating are negligible (Wunsch and Ferrari 2004), examining the depths of internal tide generation seems to be important for understanding the overturning circulation. The importance is further supported by Sandström's inference (Sandström 1908; Kuhlbrodt 2008), according to which a buoyancy-driven overturning circulation can only develop when the level of the heat source is located below the level of cold source. If we assume that the internal tide generation is the *only* energy source for maintaining the abyssal overturning circulations, the scenario of "heated from below" can be supported by an ocean basin with strong internal tide generation in the deeper part of the basin, but impeded by an ocean basin with weak internal tide generation in the deeper part of the basin.

The impact of diapycnal mixing from deep energy source for oceanic state and circulations have also been studied using more detailed scaling analysis and numerical simulations (Samelson 1998; Zhang et al. 1999). A proof of concept that not only the energy input to the internal tides matters, but also where in the vertical it is dissipated, was provided by Melet et al. (2013), who showed the sensitivity of ocean state to the vertical distributions of tidal energy fluxes above the generation sites, as parameterized by an ad hoc exponential profile of St. Laurent et al. (2002) or by a dynamically based algebraically decaying profile of Polzin (2009). These previous studies demonstrated a robust sensitivity of the ocean state and circulations to where in the vertical the ocean mixing takes place, providing strong arguments for using vertical distributions as the evaluation metric.

3. Vertical distribution of the internal tide generation

For the global ocean, the internal tide generation in STORMTIDE2 (black line, Fig. 2a) is by and large uniformly distributed with a magnitude of about 15 GW throughout the water column between 500 and 3000 m. Below 3000 m, the
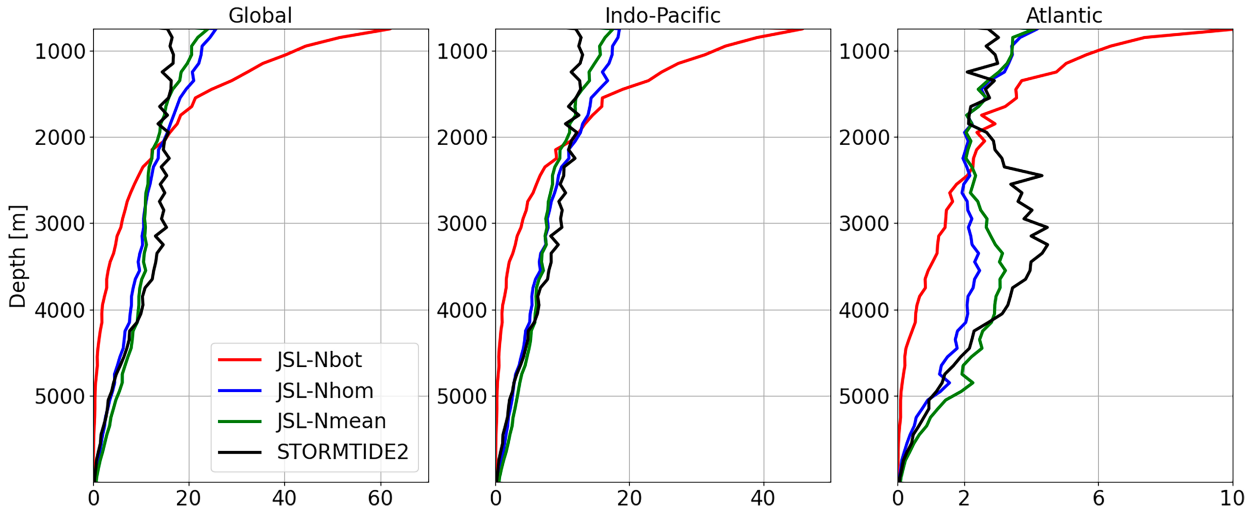
FIG. 2. Vertical profiles of internal tide generation integrated over generation sites of the same depth (left) in the global ocean, (center) in the Indo-Pacific, and (right) in the Atlantic; unit is GW (10^9 W). The profiles are derived from internal tide generation as represented by E_{LvS} (black) and by E_{JSL} using three different stratifications, namely, a homogenized stratification N_{hom} (blue), a mean stratification N_{mean} (green), and the bottom stratification N_{bot} (red). For calculating the vertical profiles, the depth is discretized using an increment of 100 m. Thus, generation sites of the same depth are sites that are located within the same 100-m-thick vertical bin.

global generation gradually decreases to zero. The nearly uniform distribution results from a compensation of completely different distributions in the Indo-Pacific and in the Atlantic: while the internal tide generation in the Indo-Pacific basin, which is stronger, decreases gradually with increasing depth throughout most part of the water column (black, middle), the internal tide generation in the Atlantic basin, though weaker, increases from about 2000 to 3000 m and reaches a maximum around 3000 m (black, right). This situation comes about since 1) the barotropic tides are much stronger in the Atlantic than in the Indo-Pacific, and 2) the major generation sites are located in a much greater depth in the Atlantic than in the Indo-Pacific. The averaged depth of the Mid-Atlantic Ridge is about 2500 m below the sea surface, whereas the hot spots found in the Pacific, such as those in the western Pacific around the Hawaiian Ridge and the Pacific archipelagos, are connected to shallow topographical structures that extend partially beyond the surface of the sea. The contrast, a decrease of internal tide generation with increasing depth in the Indo-Pacific versus a not-decreasing or even increasing internal tide generation with increasing depth in the upper 3300 m of the Atlantic, may affect the meridional overturning in the two basins differently.

To what extent the vertical distribution of internal tide generation found in E_{LvS} (black lines in Fig. 2) can be represented using the scaling relation E_{JSL} depends on the choice of N. When using the bottom stratification N_{bot} (red), a picture distinctly different from that obtained from E_{LvS} emerges: The distribution JSL-Nbot is dominated by a strong maximum in the uppermost part of the ocean, which is about 3 times stronger than the maximum obtained from E_{LvS}. Down to the ocean interior, the JSL-Nbot distribution decreases drastically with increasing depth. This leads to an extremely weak deep internal tide generation. In the global ocean and the Indo-Pacific, the internal tide generation obtained from JSL-Nbot is less than half of that obtained from E_{LvS} at about 3000 m. In the Atlantic, the deep maximum of internal tide

generation obtained from E_{LvS} is not reproduced by JSL-Nbot. That JSL-Nbot strongly overestimates the shallow internal tide generation and at the same time strongly underestimates the deep internal tide generation results from the fact that on large scales, stratification strongly decreases with depth. Consequently, using bottom stratification N_{bot} promotes the shallow internal tide generation and suppresses the deep internal tide generation disproportionately.

A much better agreement between E_{JSL} and E_{LvS} is found when using stratification throughout a large portion of the water column in case of JSL-N_{mean} (green) and JSL-N_{hom} (blue). The agreement concerns not only the maximum in the uppermost part of the ocean, which is now only slightly overestimated, but also the much more gradual decrease of the internal tide generation into the ocean interior in the global ocean and the Indo-Pacific, and the deep maximum in the Atlantic. The latter is located somewhat deeper than that obtained from E_{LvS}, but is now clearly present. Generally, the distribution JSL-N_{mean} (green) is slightly closer to that obtained from E_{LvS} than the distribution JSL-N_{hom} (blue) does.

The influence of the choice of N on the (deep) internal tide generation can be further corroborated by checking how well E_{JSL} given in Eq. (1) approximates the internal tide generation E_{LvS} based on different choices for the stratification N. For this purpose, we replace in Eq. (1) E_{JSL} by E_{LvS} and divide E_{LvS} by the topographic roughness h^2 and the squared barotropic tidal velocity $|\mathbf{U}_H|^2$ so that Eq. (1) reads $E_{\mathrm{LvS}}/(|\mathbf{U}_H|^2 h^2) \propto N$. This linear dependence on N is then checked for different expressions of N. In Fig. 3, we plot $E_{\mathrm{LvS}}/(|\mathbf{U}_H|^2 h^2)$ against the depth-averaged stratification N_{mean} (green) and the bottom stratification N_{bot} (red brown). A narrower distribution of the points around the regression lines and the higher r-squared value indicate that using N_{mean} as compared to N_{bot} in Eq. (1) is a much better approximation for the internal tide generation in STORMTIDE2, in particular,
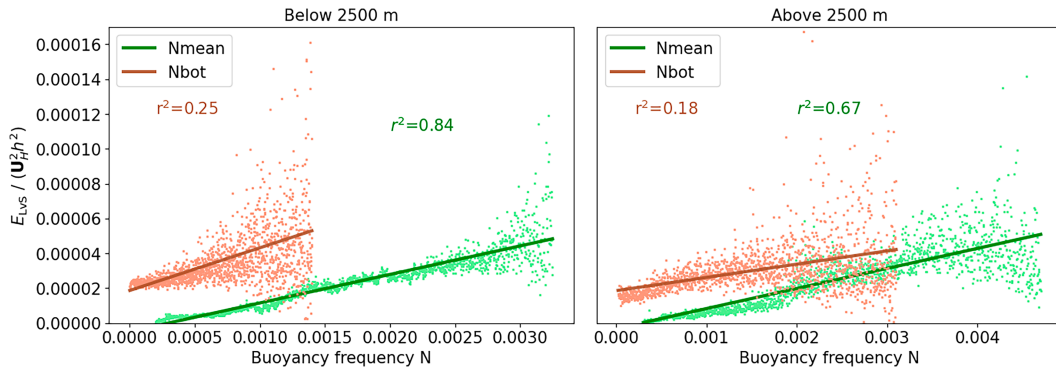
FIG. 3. Scatterplots of $E_{\text{LvS}}/(h^2\mathbf{U}_H^2)$ against the homogenized stratification N_{hom} (green) and the bottom stratification N_{bot} [(red brown) for generation sites that lie (left) below 2500 m and (right) above 2500 m. $E_{\text{LvS}}/(h^2\mathbf{U}_H^2)$ is in units of 10^{-4} kg m^{-4} s^{-1}, and N in units of 10^{-3} s^{-1}. Lines show linear regressions of the respective points. The squared correlation coefficient r^2 of these regressions is indicated in the same color as a measure for the goodness of the fit. Grid points having too-low barotropic tides (i.e., $|\mathbf{U}_H|^2 < 10^{-4}$ m^2 s^{-2}), too-small roughness (i.e., $h^2 < 10^4$ m^2), and extreme stratification with N outside the range $[N_{\min}, N_{\max}]$ are excluded from the analysis. For N_{mean}, $[N_{\min}, N_{\max}]$ is set to $[2 \times 10^{-4}, 3.25 \times 10^{-3}]$ for grid points below 2500 m and to $[3 \times 10^{-4}, 4.7 \times 10^{-3}]$ for grid points above 2500 m. For N_{bot}, $N_{\min}, N_{\max}$ is set to $[1 \times 10^{-7}, 1.4 \times 10^{-3}]$ for grid points below 2500 m and to $[2 \times 10^{-5}, 3.1 \times 10^{-3}]$ for grid points above 2500 m. The points considered sum up to 96% below 2500 m and to 90% above 2500 m.

below 2500 m, but also above. A similar picture emerges for the comparison between N_{hom} and N_{bot} (not shown).

We conclude that whether or not the vertical distribution of internal tide generation derived from E_{LvS} can be represented by E_{JSL} depends strongly on the choice of stratification used to express E_{JSL} in Eq. (1). Using only the bottom stratification strongly underestimate the deep internal tide generation. The underestimation can be quantified by the percentage of the total internal tide generation that occurs below 2500 m, which is 49% for E_{LvS} produced by STORMTIDE2. For E_{JSL}, this percentage is about 47% and 41% when using stratification characteristic for a large part of the water column (N_{mean} and N_{hom}), but only 15% when using the bottom stratification (N_{bot}). The next section discusses the consequence of underestimating deep internal tide generation.

4. Water mass transformation

The water mass transformation analysis goes back to Walin (1982) and was recently used to connect abyssal mixing and overturning (de Lavergne et al. 2016; Ferrari et al. 2016; Callies and Ferrari 2018; Drake et al. 2020). When quantifying the mixing resulting from the energy available from internal tide generation by a three-dimensional diffusivity κ_v, we can translate the effect of this mixing into water mass transformation rate or dianeutral transport T defined as

$$T = -\partial_\gamma \int_{A_\gamma} F^\gamma \, dA, \qquad (3)$$

where γ is the neutral density (Jackett and McDougall 1997), $F^\gamma = -\kappa_v \partial_z \gamma$ is the vertical flux of neutral density through a neutral density surface, and A_γ indicates the surface of a constant neutral density γ. The γ and $\partial_z \gamma$ are taken from the time-mean state of STORMTIDE2. We neglect nonlinear effects in the equation of state for the sake of simplicity, even though they can

impact the water mass transformation budget due to cabbeling and thermobaricity (Groeskamp et al. 2016). Furthermore, by computing the density flux via the z derivative instead of using the dianeutral derivative, it assumes that neutral density surfaces are nearly horizontal in the abyssal ocean. Ferrari et al. (2016) argues that this is indeed justified. We integrate Eq. (3) from 30°S to 48°N, since de Lavergne et al. (2016) find that considering the area between 30°S and 48°N is a good approximation of the overturning streamfunction at 30°S.

To obtain κ_v, we choose the simplest approach and assume that κ_v results from near-field mixing (St. Laurent et al. 2002), i.e., from the portion of the high-mode internal tides, that dissipate near the generation sites. We consider this assumption as adequate, since our usage of the water mass transformation framework serves only to illustrate the importance of the above mentioned deep internal tide generation, rather than to provide quantitative information on the abyssal overturning related with the deep internal tide generation. Under the near-field mixing assumption, κ_v is parameterized by

$$\kappa_v = \frac{\Gamma q E \mathcal{F}(z)}{\rho N^2}, \qquad (4)$$

where E equals either E_{LvS} or E_{JSL}, q is the dissipation efficiency which is set to the widely used value of 0.3 (St. Laurent et al. 2002), $\Gamma = 0.2$ is the canonical value for mixing efficiency (Osborn 1980), N is the buoyancy frequency at the generation site, ρ is density, and

$$\mathcal{F}(z) = \frac{e^{(-H+z)/\zeta}}{\zeta(1 - e^{-H/\zeta})} \qquad (5)$$

is an exponential decay of the mixing strength from the bottom upward with a decay scale $\zeta = 500$ m and the water depth H.
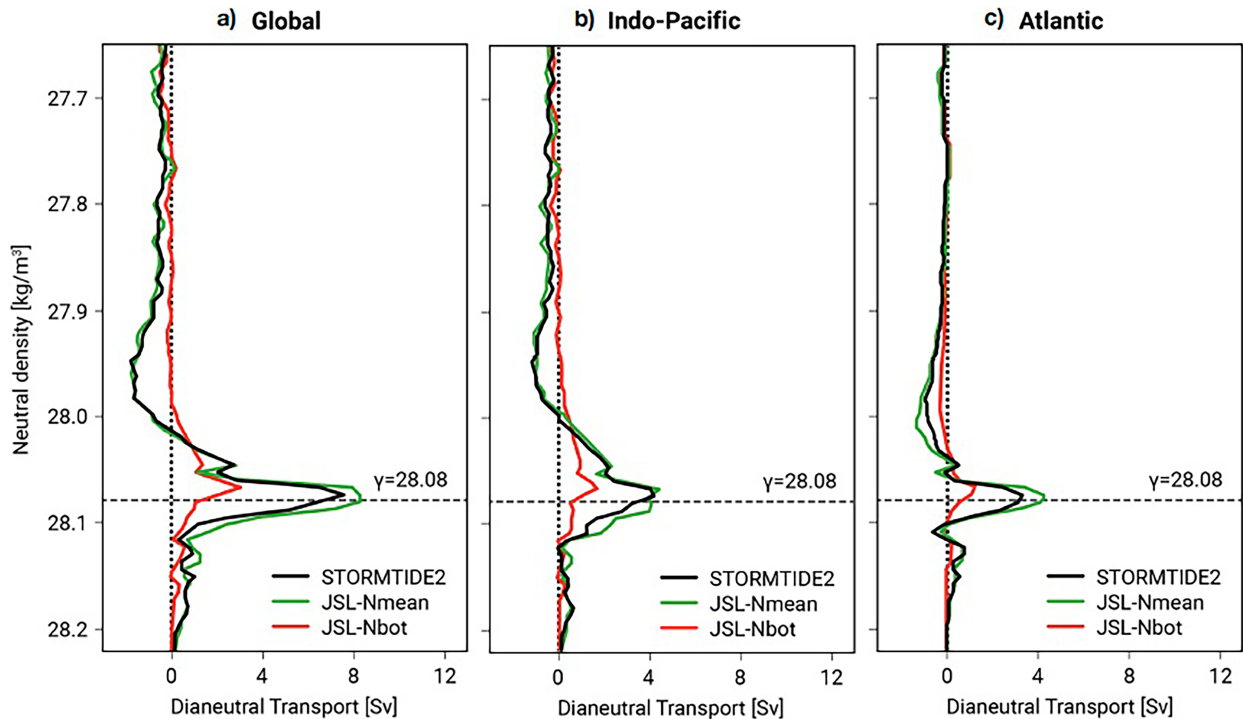
FIG. 4. Water mass transformation due to diapycnal density fluxes between 30°S and 48°N (a) in the global ocean and divided into (b) the Indo-Pacific and (c) the Atlantic Oceans. This latitude band was also chosen in de Lavergne et al. (2017) because most of the AABW created in the Southern Ocean is expected to upwell diabatically here. Water mass transformation is computed in density space with bin size of 0.007 kg m^{-3}. Colors match the different internal tide generation estimates from Fig. 2.

De Lavergne et al. (2017) nicely show that the maximum of the upward dianeutral transport occurs in the density class that occupies the largest part of the ocean seafloor because there the most mixing-induced lightening occurs. The dianeutral transport rate in this density class is indicative of how much tidal mixing can contribute to the upwelling of dense water in the abyssal ocean. In STORMTIDE2 (black, Fig. 4), this is at $\gamma = 28.08$ kg m^{-3}, very close to the value of $\gamma = 28.1$ kg m^{-3} from de Lavergne et al. (2017, 2016). The water mass transformation in the densest density class is an upwelling (positive) close to 8 Sv (1 Sv $\equiv 10^6$ m^3 s^{-1}) in the global ocean. About half of this 8 Sv is generated in the Indo-Pacific (middle, black curve) and the other half is generated in the Atlantic (right, black curve). The comparably large water mass transformation related to the densest water masses in the Atlantic is, at least partially, due to the stronger deep internal tide generation in the Atlantic than in the Indo-Pacific.

There are two other differences between water mass transformation rates in the two ocean basins, which are likely more strongly influenced by the different spatial distribution of neutral density in the two basins than by the different distributions of κ_v. First, while the Indo-Pacific shows upwelling water masses (i.e., positive water mass transformation) covering a broad density range of 0.15 kg m^{-3} from 28.15 to 28 kg m^{-3}, this density range of upwelling water in the Atlantic is only 0.03 kg m^{-3} covering from 28.1 to 28.07 kg m^{-3}. This difference reflects the larger vertical extent of the Indo-Pacific AABW overturning cell than that of the Atlantic AABW cell confined to depth between 5 and 3 km (Lumpkin and Speer 2007). Second, the

compensating downwelling (negative water mass transformation) occurs in lighter density classes in the Indo-Pacific than in the Atlantic. While the downwelling water masses have a density around $27.9 < \gamma < 28.0$ in the Indo-Pacific, the downwelling water masses in the Atlantic are denser and have a density around $27.95 < \gamma < 28.05$.

Like for the vertical distribution of the internal tide generation, to what extent the water mass transformation rates obtained from E_{JSL} is consistent with that obtained from E_{LvS} (black) depends on the stratification used. The rate obtained from E_{JSL} is comparable to that obtained from E_{LvS} when using depth-averaged stratification N_{mean} (green), but much too small when using the bottom stratification N_{bot} (red). For the densest water mass class, the water mass transformation rate is more than 50% smaller when using N_{bot} than when using N_{mean}. Like in the vertical distribution of the internal tide generation (Fig. 2), JSL-N_{hom} produces water mass transformation rates very similar to that obtained from JSL-N_{mean} (not shown).

The water mass transformation analysis underlines what we saw in the vertical distribution of the internal tide generation rates: considering the density over a large portion of the water column (JSL-N_{mean}) leads to larger upwelling rates than considering only the bottom stratification (JSL-N_{bot}) does. The STORMTIDE2 water mass transformation can be properly reproduced using the depth-averaged stratification as in JSL-N_{mean} (or JSL-N_{hom}) but not reproduced using the bottom stratification only as in JSL-N_{bot}.
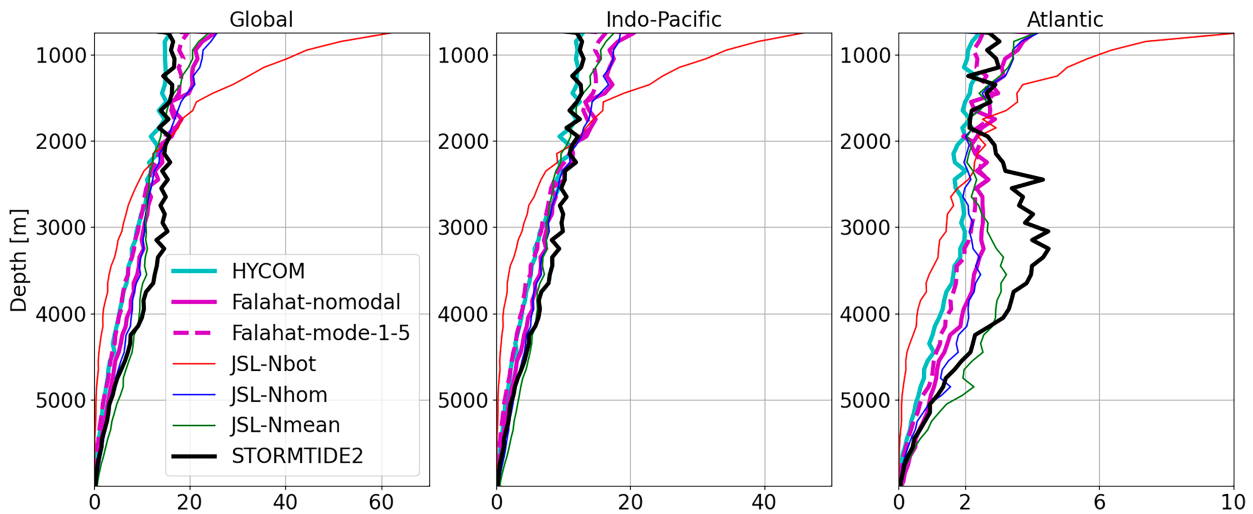
FIG. 5. Vertical profiles of E_{LvS} (black; same as black lines in Fig. 2); the internal tide generation simulated by HYCOM (Buijsman et al. 2020) (cyan); the internal tide generation derived from linear wave theory (Falahat et al. 2014) without a modal decomposition following Nycander (2005) (solid magenta) and with a modal decomposition for the first five modes (dashed magenta); and vertical profiles of E_{JSL} (thin lines) obtained using the bottom stratification N_{bot} (red), a homogenized stratification N_{hom} (blue), and a mean stratification N_{mean} (blue). The cyan lines are calculated using data downloaded from https://zenodo.org/record/6478745#.Yp95dqQpA0E; the magenta lines are calculated using data downloaded from https://www.seanoe.org/data/00470/58153/.

5. Discussion

a. Comparison of E_{LvS} with other estimates of internal tide generation

The results shown in sections 3 and 4 are obtained by comparing E_{JSL} with E_{LvS} within the framework of STORMTIDE2. A question naturally arises is how realistic is E_{LvS}. Clearly, this question cannot be definitively answered due to the lack of the ground truth for internal tide generation. Nevertheless, the question can be approached by considering the range covered by available estimates. This range can then be used to quantify the uncertainty in our present knowledge about internal tide generation. The result of previous sections would become more significant if E_{JSL} expressed in terms of N_{hom} and N_{mean} lies inside, whereas E_{JSL} expressed in terms of N_{bot} lies outside this range.

There exist two types of estimates for internal tide generation. One relies on semianalytical solutions of linear wave equations; the other type relies on numerical simulation of a global general circulation model. As pointed out in section 1, the two types suffer from different shortcomings. Below, we compare four estimates of M_2 internal tide generation, including apart from E_{LvS} the estimates obtained from semianalytical solutions by Falahat et al. (2014) [both without a modal decomposition following Nycander (2005) and with a modal decomposition] and the internal tide generation obtained from a realistic HYCOM simulation by Buijsman et al. (2020). For the estimates based on modal decomposition (Falahat et al. 2014; Buijsman et al. 2020), internal tide generation by the first five modes is considered. Even though MPIOM resolves only two to three modes, we consider all four estimates as being representative for the total internal tide generation. Note that HYCOM and MPIOM are two different ocean models. While MPIOM uses a z coordinate, HYCOM uses a hybrid

vertical coordinate. Although both use a tripolar grid, the horizontal resolution is finer in HYCOM (about 4 km) than in MPIOM (about 10 km). A discussion on differences among these estimates is beyond the scope of this paper. We concentrate here on the range covered by the four estimates only.

The vertical profiles of E_{LvS} (black in Fig. 5) and of the estimates of Falahat et al. (2014) (dashed and solid magenta lines) and Buijsman et al. (2020) (cyan lines) show a common feature that internal tide generation decreases less strongly with increasing depth in the Atlantic (right) than in the Indo-Pacific (middle). However, there are also some differences. In particular, the Atlantic maximum at about 3000 m found in E_{LvS} (black) is hardly noticeable in the HYCOM estimate (cyan) and almost not present in the estimates by Falahat et al. (2014) (magenta).

When considering the range covered by the black, cyan, and magenta lines as the range of uncertainty in estimating the true internal tide generation, Fig. 5 shows that E_{JSL} calculated using N_{mean} or N_{hom} lies essentially inside this range, whereas E_{JSL} calculated using N_{bot} lies essentially outside this range. In particular, using N_{bot} leads to a vertical profile that has values larger than the range of four estimates in the upper oceans above 2000 m and smaller than this range in the deep oceans below 2000 m. We hence conclude that the underestimation of deep internal tide generation and the deep water mass transformation obtained using JSL-N_{bot} in sections 3 and 4 is significant with respect to the range of the four considered estimates.

b. Relevance of dependence on N for near-field tidal mixing

The parameterization of St. Laurent et al. (2002) relies on the energy flux from barotropic tides to high-mode internal tides and represents only near-field tidal mixing. High modes are prone to
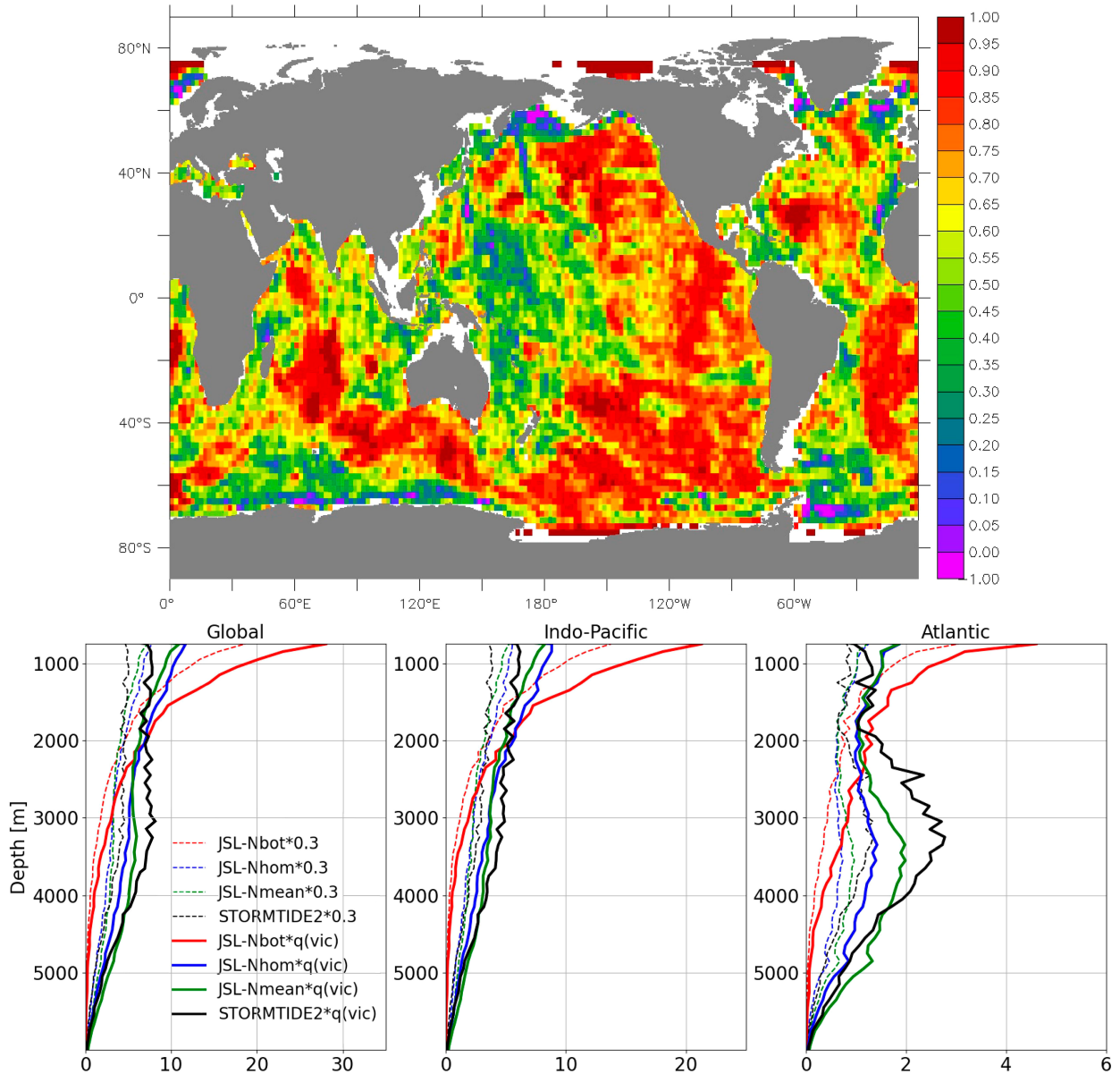
FIG. 6. (top) Geographical distribution of dissipation efficiency q from Vic et al. (2019) (courtesy of Clément Vic) and (bottom) the vertical profiles of high-mode internal tide generation qE (left) in the global ocean, (center) in the Indo-Pacific, and (right) in the Atlantic. The profiles are derived from internal tide generation represented by E_{LvS} (black) and by E_{JSL} using a mean stratification N_{mean} (green), a homogenized stratification N_{hom} (blue), and the bottom stratification N_{bot} (red) with the geographically varying q shown in the top panel (solid lines) and $q = 0.3$ (dashed lines).

breaking and can hence provide energy for mixing near the generation sites. This behavior of high modes differs strongly from that of low modes, which tend to propagate away from the generation sites and provide only energy for far-field background mixing. Following this general understanding, a key ingredient of a near-field tidal mixing parameterization should be a geographical map of the high-mode internal tide generation, rather than that of the total internal tide generation, which is dominated by that of low-mode generation. However, the high-mode generation is more difficult to estimate than the total generation. Apart from

the study by Vic et al. (2019), which is dedicated to the high-mode generation with the highest resolved mode being about 50, most estimates based on linear wave theory concentrate on the generation of lower modes or the total generation of all modes (Nycander 2005; Falahat et al. 2014). When using state-of-the-art high-resolution numerical models, only the low-mode generation can be captured. The approach to deal with this problem, originally proposed by St. Laurent et al. (2002), is to multiply the total generation with a local dissipation efficiency q, defined as the fraction of the high-mode generation to the total generation.

Following this approach, *both* the total generation *and* the local dissipation efficiency q needs to be accurately estimated. The question arises then is whether the sensitivity of E_{JSL} to stratification N, which was identified in the previous sections, still remains relevant when taking the more realistic spatially varying efficiency q from Vic et al. (2019), reproduced in Fig. 6 (top), into account. A positive answer to the question would further confirm the need to use depth-averaged stratification (as opposed to bottom stratification) for adequately representing the true near-field tidal mixing.

To answer this question, we consider the vertical profiles of high-mode internal tide generation qE (Fig. 6, bottom), obtained using the geographically varying q from Vic et al. (2019) (solid lines) and those obtained using geographically constant $q = 0.3$ (dashed lines). The latter profiles have the same shapes as the corresponding lines in Fig. 2, albeit the magnitudes are reduced by factor 0.3. Apart from the result that stronger high-mode energy fluxes are obtained using q from Vic et al. (2019) than using $q = 0.3$, the overall shapes of the vertical profiles of qE follow essentially those of E. The shortcoming of using N_{bot} that the deep generation is strongly underestimated, especially in the Atlantic, prevails or is even further enhanced when using the geographically varying q relative to using $q = 0.3$.

The further enhancement comes about, since the dissipation efficiency derived by Vic et al. (2019) tends to be large at the deeper sites and small at the shallower sites (Fig. 6). Thus, multiplying a map of internal tide generation by this distribution of dissipation efficiency emphasizes the deep internal tide generation. In the Atlantic, the major generation sites are located over the Mid-Atlantic Ridge. A large part of them are deep sites located around 2500–3000 m, whereas a small part are shallower sites, e.g., the sites near the Azores and Canary Islands and the Walvis Ridge. The values of the dissipation efficiency are in the range of 0.8–1.0 over the deep sites, partially due to the abyssal hills there, but about 0.1–0.3 over the shallower sites. Multiplied with this distribution of dissipation efficiency q, rather than with a constant $q = 0.3$, the maximum of internal tide generation at about 2500–3500 m is further enhanced.

In the Pacific, dissipation efficiency q has small values in the range 0.2–0.5 in the western part of the Pacific, e.g., at the shallow sites over the Hawaiian Ridge and topographic features around Pacific archipelagos where the amount of the total internal tide generation is large, and large values in the range of 0.8–1.0 at deep sites over east Pacific Rise where the total internal tide generation is more than one to two *orders* of magnitudes weaker than that in the western Pacific. Due to the extremely low internal tide generation, the large values of q in the eastern Pacific have little impact on the overall vertical distribution of in the Pacific.

The above consideration suggests that taking the more realistic spatially varying dissipation efficiency q into account can enhance the difference between the available energy source for tidal mixing in the upper part of the Atlantic and that in the deep Atlantic. This may further strengthen the impact of deep tidal mixing on the deep overturning circulations (Cimoli et al. 2023).

6. Summary

The parameterization of tidal mixing is often implemented based on E_{JSL}, a simple scaling relation for internal tide generation (Jayne and St. Laurent 2001). Together with the local dissipation efficiency q, E_{JSL} determines the amount of internal-tide generation that can be made available for near-field tidal mixing and is used in the mixing parameterization by St. Laurent et al. (2002). Here we evaluate the scaling relation E_{JSL} against E_{LvS}, a three-dimensional map of the internal tide generation simulated by an ocean GCM (Li and von Storch 2020).

We found that the internal tide generation described by E_{JSL} depends strongly on the buoyancy frequency N used to calculate E_{JSL} and this dependence has a strong impact on deep water mass transformation. E_{JSL} is not comparable to E_{LvS} and produces strongly reduced deep water mass transport when calculated using buoyancy frequency at the seafloor N_{bot}, as it is commonly done. E_{JSL} becomes comparable to E_{LvS} and produces similar deep water mass transformation as E_{LvS}, when calculated using buoyancy frequency N_{mean} or N_{hom} obtained by averaging N over a large portion of the water column. Using N_{bot} instead of N_{mean} and N_{hom} leads to too-strong internal tide generation in the upper ocean, and at the same time, too-weak internal tide generation in the deep ocean. Moreover, the different vertical distributions in the different ocean basins, characterized by a generally decreasing internal tide generation with increasing depth in the Indo-Pacific but not-decreasing or even increasing internal tide generation with increasing depth in the upper 3000 m of the Atlantic found in E_{LvS} can only be reproduced when using N_{mean} or N_{hom}, not when using N_{bot}. Relative to E_{LvS}, the overestimation in the upper ocean and the underestimation in the deep ocean obtained from E_{JSL} with N_{bot} easily amount to more than 50% of the internal tide generation described by E_{LvS}. Similar over- and underestimation are obtained when compared to the range covered by E_{LvS} together with three other estimates of internal tide generation. Taking the more realistic local dissipation efficiency q (Vic et al. 2019) into account, which tends to have larger values at deep generation sites than at shallow generation sites, further emphasizes the strong deep internal tide generation, which cannot be reproduced using E_{LvS} with N_{bot}.

The sensitivity of E_{JSL} to stratification and its implication for water mass transformation identified in this study suggest that the tidal mixing parameterization of St. Laurent et al. (2002) can be easily improved by replacing the common practice of calculating E_{JSL} using bottom stratification N_{bot} by using a depth-averaged stratification N_{mean}.

Data availability statement. A description of the simulation and the scripts used to produce the main results of this paper is

archived in the publication repository of the Max Planck Society under https://hdl.handle.net/21.11116/0000-000C-DB09-4.

REFERENCES

Arbic, B. K., S. T. Garner, R. W. Hallberg, and H. L. Simmons, 2004: The accuracy of surface elevations in forward global barotropic and baroclinic tide models. *Deep-Sea Res. II*, **51**, 3069–3101, https://doi.org/10.1016/j.dsr2.2004.09.014.

——, A. J. Wallcraft, and E. J. Metzger, 2010: Concurrent simulation of the eddying general circulation and tides in a global ocean model. *Ocean Modell.*, **32**, 175–187, https://doi.org/10.1016/j.ocemod.2010.01.007.

Bell, T. H., 1975: Lee waves in stratified flows with simple harmonic time dependence. *J. Fluid Mech.*, **67**, 705–722, https://doi.org/10.1017/S0022112075000560.

Brüggemann, N., and Coauthors, 2023: Parameterized internal wave mixing in three ocean general circulation models. *ESS Open Archive*, https://doi.org/10.22541/essoar.168286764.45506774/v1.

Buijsman, M. C., and Coauthors, 2020: On the interplay between horizontal resolution and wave drag and their effect on tidal baroclinic mode waves in realistic global ocean simulations. *Ocean Modell.*, **152**, 101656, https://doi.org/10.1016/j.ocemod.2020.101656.

Callies, J., and R. Ferrari, 2018: Dynamics of an abyssal circulation driven by bottom-intensified mixing on slopes. *J. Phys. Oceanogr.*, **48**, 1257–1282, https://doi.org/10.1175/JPO-D-17-0125.1.

Cimoli, L., and Coauthors, 2023: Significance of diapycnal mixing within the Atlantic Meridional Overturning Circulation. *AGU Adv.*, **4**, e2022AV000800, https://doi.org/10.1029/2022AV000800.

Danabasoglu, G., S. C. Bates, B. P. Briegleb, S. R. Jayne, M. Jochum, W. G. Large, S. Peacock, and S. G. Yeager, 2012: The CCSM4 ocean component. *J. Climate*, **25**, 1361–1389, https://doi.org/10.1175/JCLI-D-11-00091.1.

de Lavergne, C., G. Madec, J. Le Sommer, A. J. Nurser, and A. C. Naveira Garabato, 2016: On the consumption of Antarctic Bottom Water in the abyssal ocean. *J. Phys. Oceanogr.*, **46**, 635–661, https://doi.org/10.1175/JPO-D-14-0201.1.

——, ——, F. Roquet, R. M. Holmes, and T. J. McDougall, 2017: Abyssal ocean overturning shaped by seafloor distribution. *Nature*, **551**, 181–186, https://doi.org/10.1038/nature24472.

——, S. Falahat, G. Madec, F. Roquet, J. Nycander, and C. Vic, 2019: Toward global maps of internal tide energy sinks. *Ocean Modell.*, **137**, 52–75, https://doi.org/10.1016/j.ocemod.2019.03.010.

Drake, H. F., R. Ferrari, and J. Callies, 2020: Abyssal circulation driven by near-boundary mixing: Water mass transformations and interior stratification. *J. Phys. Oceanogr.*, **50**, 2203–2226, https://doi.org/10.1175/JPO-D-19-0313.1.

Dunne, J. P., and Coauthors, 2012: GFDL'S ESM2 global coupled climate–carbon Earth system models. Part I: Physical formulation and baseline simulation characteristics. *J. Climate*, **25**, 6646–6665, https://doi.org/10.1175/JCLI-D-11-00560.1.

Exarchou, E., J. S. Von Storch, and J. H. Jungclaus, 2012: Impact of tidal mixing with different scales of bottom roughness on the general circulation. *Ocean Dyn.*, **62**, 1545–1563, https://doi.org/10.1007/s10236-012-0573-1.

Falahat, S., J. Nycander, F. Roquet, and M. Zarroug, 2014: Global calculation of tidal energy conversion into vertical normal modes. *J. Phys. Oceanogr.*, **44**, 3225–3244, https://doi.org/10.1175/JPO-D-14-0002.1.

Farr, T. G., and Coauthors, 2007: The Shuttle Radar Topography Mission. *Rev. Geophys.*, **45**, RG2004, https://doi.org/10.1029/2005RG000183.

Ferrari, R., A. Mashayek, T. J. McDougall, M. Nikurashin, and J.-M. Campin, 2016: Turning ocean mixing upside down. *J. Phys. Oceanogr.*, **46**, 2239–2261, https://doi.org/10.1175/JPO-D-15-0244.1.

Gent, P. R., and J. C. McWilliams, 1990: Isopycnal mixing in ocean circulation models. *J. Phys. Oceanogr.*, **20**, 150–155, https://doi.org/10.1175/1520-0485(1990)020<0150:IMIOCM>2.0.CO;2.

Groeskamp, S., R. P. Abernathey, and A. Klocker, 2016: Water mass transformation by cabbeling and thermobaricity. *Geophys. Res. Lett.*, **43**, 10835–10845, https://doi.org/10.1002/2016GL070860.

Jackett, D. R., and T. J. McDougall, 1997: A neutral density variable for the world's oceans. *J. Phys. Oceanogr.*, **27**, 237–263, https://doi.org/10.1175/1520-0485(1997)027<0237:ANDVFT>2.0.CO;2.

Jayne, S. R., 2009: The impact of abyssal mixing parameterizations in an ocean general circulation model. *J. Phys. Oceanogr.*, **39**, 1756–1775, https://doi.org/10.1175/2009JPO4085.1.

——, and L. C. St. Laurent, 2001: Parameterizing tidal dissipation over rough topography. *Geophys. Res. Lett.*, **28**, 811–814, https://doi.org/10.1029/2000GL012044.

Jungclaus, J. H., and Coauthors, 2013: Characteristics of the ocean simulations in the Max Planck Institute Ocean Model (MPIOM) the ocean component of the MPI-Earth system model. *J. Adv. Model. Earth Syst.*, **5**, 422–446, https://doi.org/10.1002/jame.20023.

Kuhlbrodt, T., 2008: On Sandström's inferences from his tank experiments: A hundred years later. *Tellus*, **60A**, 819–830, https://doi.org/10.1111/j.1600-0870.2008.00357.x.

Li, Z., and J. S. von Storch, 2020: M_2 internal-tide generation in STORMTIDE2. *J. Geophys. Res. Oceans*, **125**, e2019JC015453, https://doi.org/10.1029/2019JC015453.

——, ——, and M. Müller, 2015: The M_2 internal tide simulated by a 1/10° OGCM. *J. Phys. Oceanogr.*, **45**, 3119–3135, https://doi.org/10.1175/JPO-D-14-0228.1.

——, J.-S. von Storch, and M. Müller, 2017: The K_1 internal tide simulated by a 1/10° OGCM. *Ocean Modell.*, **113**, 145–156, https://doi.org/10.1016/j.ocemod.2017.04.002.

Llewellyn Smith, S. G., and W. R. Young, 2002: Conversion of the barotropic tide. *J. Phys. Oceanogr.*, **32**, 1554–1566, https://doi.org/10.1175/1520-0485(2002)032<1554:COTBT>2.0.CO;2.

Lumpkin, R., and K. Speer, 2007: Global ocean meridional overturning. *J. Phys. Oceanogr.*, **37**, 2550–2562, https://doi.org/10.1175/JPO3130.1.

Madec, G., and NEMO Team, 2016: NEMO ocean engine, version 3.6. Note du Pôle de modélisation de l'Institut Pierre-Simon Laplace 27, 386 pp., https://www.nemo-ocean.eu/wp-content/uploads/NEMO_book.pdf.

Melet, A., R. Hallberg, S. Legg, and K. Polzin, 2013: Sensitivity of the ocean state to the vertical distribution of internal-tide-driven mixing. *J. Phys. Oceanogr.*, **43**, 602–615, https://doi.org/10.1175/JPO-D-12-055.1.

Müller, M., J. Y. Cherniawsky, M. G. Foreman, and J. S. Von Storch, 2012: Global M_2 internal tide and its seasonal variability from high resolution ocean circulation and tide modeling. *Geophys. Res. Lett.*, **39**, L19607, https://doi.org/10.1029/2012GL053320.

Munk, W., and C. Wunsch, 1998: Abyssal recipes II: Energetics of tidal and wind mixing. *Deep-Sea Res. I*, **45**, 1977–2010, https://doi.org/10.1016/S0967-0637(98)00070-3.

Munk, W. H., 1966: Abyssal recipes. *Deep-Sea Res. Oceanogr. Abstr.*, **13**, 707–730, https://doi.org/10.1016/0011-7471(66)90602-4.

Nielsen, S. B., M. Jochum, C. Eden, and R. Nuterman, 2018: An energetically consistent vertical mixing parameterization in CCSM4. *Ocean Modell.*, **127**, 46–54, https://doi.org/10.1016/j.ocemod.2018.03.002.

Nycander, J., 2005: Generation of internal waves in the deep ocean by tides. *J. Geophys. Res.*, **110**, C10028, https://doi.org/10.1029/2004JC002487.

Olbers, D., and C. Eden, 2013: A global model for the diapycnal diffusivity induced by internal gravity waves. *J. Phys. Oceanogr.*, **43**, 1759–1779, https://doi.org/10.1175/JPO-D-12-0207.1.

Osborn, T. R., 1980: Estimates of the local rate of vertical diffusion from dissipation measurements. *J. Phys. Oceanogr.*, **10**, 83–89, https://doi.org/10.1175/1520-0485(1980)010<0083:EOTLRO>2.0.CO;2.

Pacanowski, R. C., and S. G. H. Philander, 1981: Parameterization of vertical mixing in numerical models of tropical oceans. *J. Phys. Oceanogr.*, **11**, 1443–1451, https://doi.org/10.1175/1520-0485(1981)011<1443:POVMIN>2.0.CO;2.

Pollmann, F., and J. Nycander, 2023: Resolving the horizontal direction of internal tide generation: Global application for the M_2 tide's first mode. *J. Phys. Oceanogr.*, **53**, 1251–1267, https://doi.org/10.1175/JPO-D-22-0144.1.

Polzin, K. L., 2009: An abyssal recipe. *Ocean Modell.*, **30**, 298–309, https://doi.org/10.1016/j.ocemod.2009.07.006.

Redi, M., 1982: Oceanic isopycnal mixing by coordinate rotation. *J. Phys. Oceanogr.*, **12**, 1154–1158, https://doi.org/10.1175/1520-0485(1982)012<1154:OIMBCR>2.0.CO;2.

Samelson, R. M., 1998: Large-scale circulation with locally enhanced vertical mixing. *J. Phys. Oceanogr.*, **28**, 712–726, https://doi.org/10.1175/1520-0485(1998)028<0712:LSCWLE>2.0.CO;2.

Sandström, J., 1908: Dynamische versuche mit meerwasser. *Ann. Hydrogr. Marit. Meteor.*, **36**, 6–23.

Sasaki, H., and Coauthors, 2020: A global eddying hindcast ocean simulation with OFES2. *Geosci. Model Dev.*, **13**, 3319–3336, https://doi.org/10.5194/gmd-13-3319-2020.

Simmons, H. L., S. R. Jayne, L. C. St. Laurent, and A. J. Weaver, 2004: Tidally driven mixing in a numerical model of the ocean general circulation. *Ocean Modell.*, **6**, 245–263, https://doi.org/10.1016/S1463-5003(03)00011-8.

St. Laurent, L. C., H. L. Simmons, and S. R. Jayne, 2002: Estimating tidally driven mixing in the deep ocean. *Geophys. Res. Lett.*, **29**, 2106, https://doi.org/10.1029/2002GL015633.

Thomas, M., J. Sündermann, and E. Maier-Reimer, 2001: Consideration of ocean tides in an OGCM and impacts on subseasonal to decadal polar motion excitation. *Geophys. Res. Lett.*, **28**, 2457–2460, https://doi.org/10.1029/2000GL012234.

Vic, C., and Coauthors, 2019: Deep-ocean mixing driven by small-scale internal tides. *Nat. Commun.*, **10**, 2099, https://doi.org/10.1038/s41467-019-10149-5.

Walin, G., 1982: On the relation between sea-surface heat flow and thermal circulation in the ocean. *Tellus*, **34**, 187–195, https://doi.org/10.3402/tellusa.v34i2.10801.

Wunsch, C., and R. Ferrari, 2004: Vertical mixing, energy, and the general circulation of the oceans. *Annu. Rev. Fluid Mech.*, **36**, 281–314, https://doi.org/10.1146/annurev.fluid.36.050802.122121.

Zarroug, M., J. Nycander, and K. Döös, 2010: Energetics of tidally generated internal waves for nonuniform stratification. *Tellus*, **62A**, 71–79, https://doi.org/10.1111/j.1600-0870.2009.00415.x.

Zhang, J., R. W. Schmitt, and R. X. Huang, 1999: The relative influence of diapycnal mixing and hydrologic forcing on the stability of the thermohaline circulation. *J. Phys. Oceanogr.*, **29**, 1096–1108, https://doi.org/10.1175/1520-0485(1999)029<1096:TRIODM>2.0.CO;2.